Electronic Supplementary Information (ESI)

Orchestrated Spatial Confinement and Phase Engineering with SDS for Air-Stable and High-Rate Alluaudite Sodium-Ion Cathodes

Ye Tao,[a] Fangzhou Zhao,[a] Yuqi Zhou,[a] Weijian Wang,[a] Wanglai Cen,[a] Jianyong Wang,[b] Xinglin Tang,[c] Ting Wang,[c] Xiaodong Hu,[d] and Yongzhi Zhang[a]*

[a.] Institute of New Energy and Low-Carbon Technology (INELT), Sichuan University, Chengdu 610065, China

[b.] State Key Laboratory of Advanced Chemical Power Sources, Guizhou Meiling Power Sources Co. Ltd., Zunyi 563003, China

[c.] School of Chemical Engineering, Sichuan University, Chengdu 610065, China.

[d.] College of New Energy and Materials, Leshan Vocational and Technical College, Leshan 614000, China

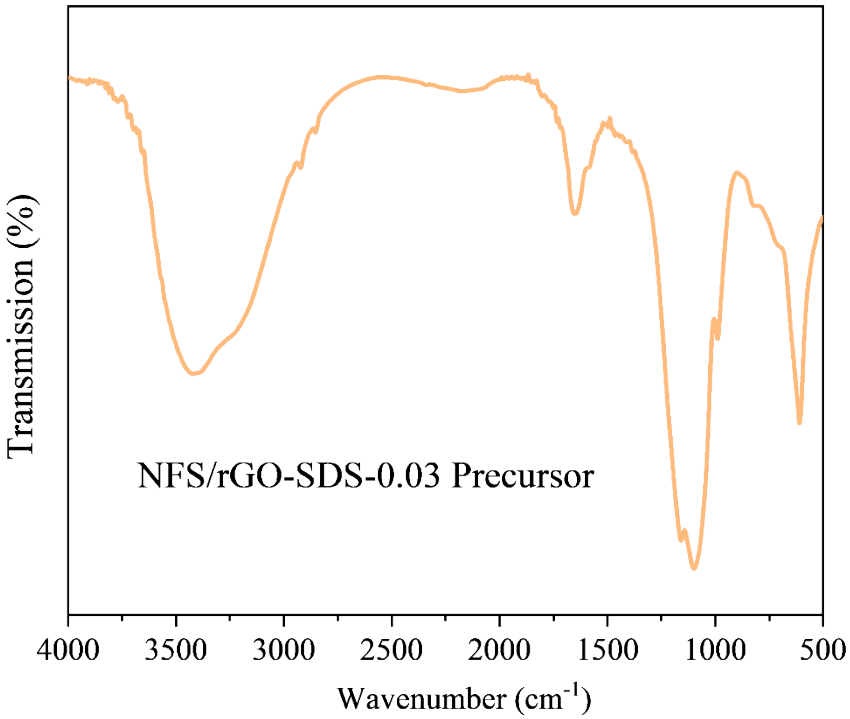

Fig. S1. FT-IR spectrum of the NFS/rGO-SDS-0.03 precursor.

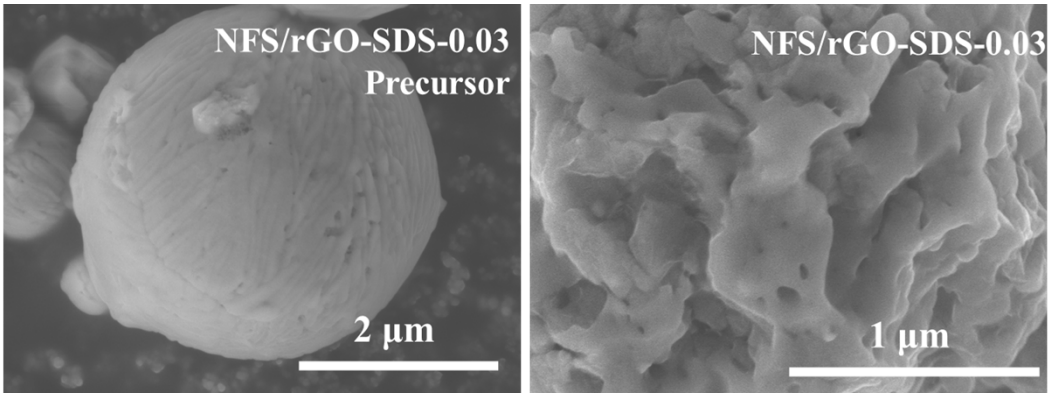

Fig. S2. SEM images of the NFS/rGO-SDS-0.03 precursor and sintered samples.

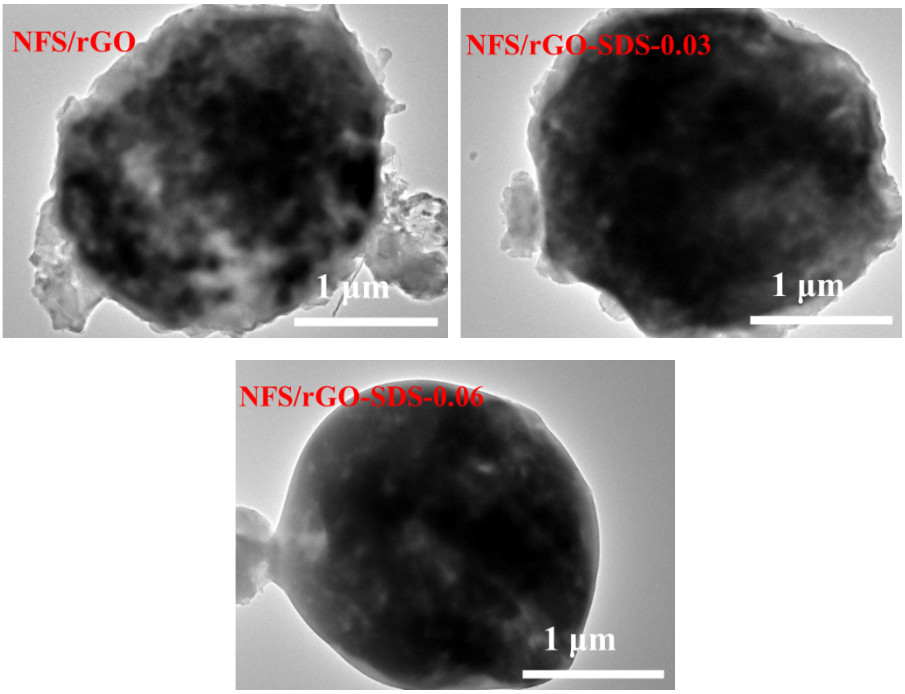

Fig. S3. TEM images of NFS/rGO-SDS-*x*. (*x*=0, 0.03, 0.06)

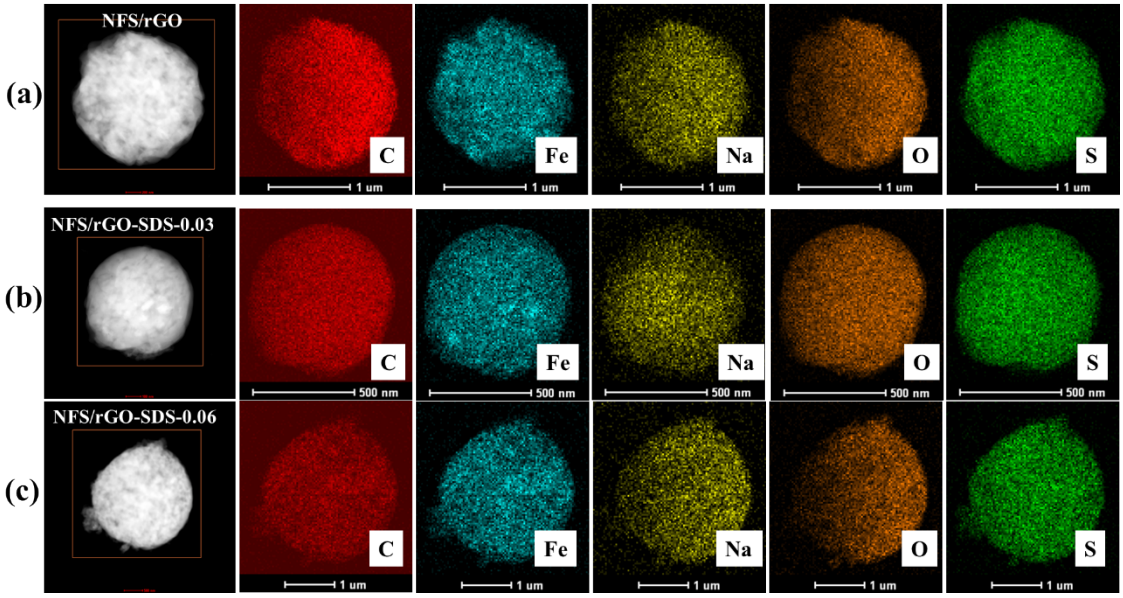

Fig. S4. TEM images and EDS elemental mapping of NFS/rGO-SDS-*x*. (*x*=0, 0.03, 0.06)

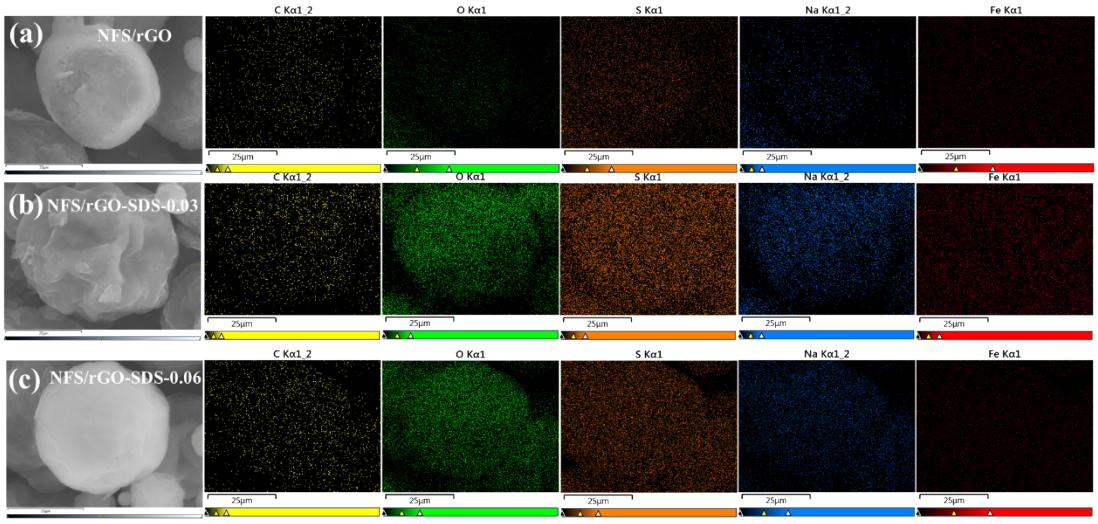

Fig. S5. SEM images and EDS elemental mapping of NFS/rGO-SDS-*x*. (*x*=0, 0.03, 0.06)

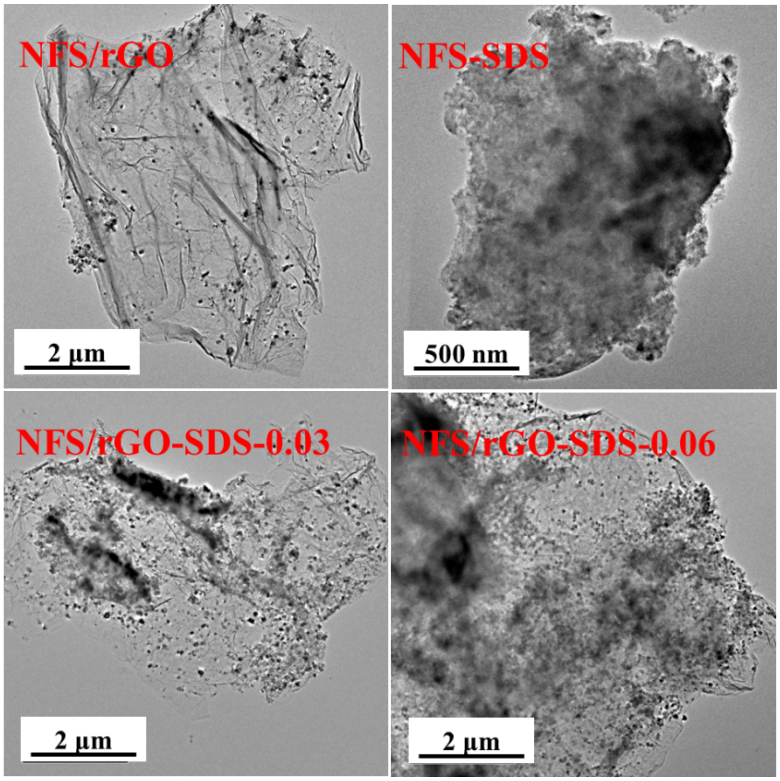

Fig. S6. TEM images of the acid-washed samples.

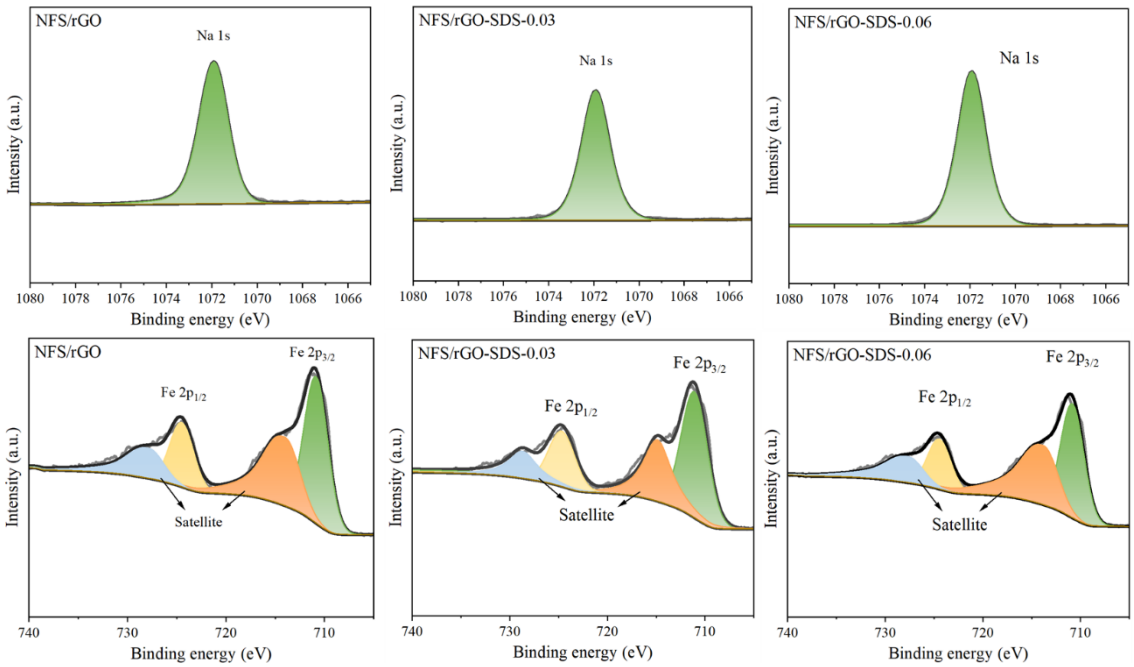

Fig. S7. High-resolution XPS spectra of Na 1s and Fe 2p for NFS/rGO-SDS-*x*. (*x*=0, 0.03, 0.06)

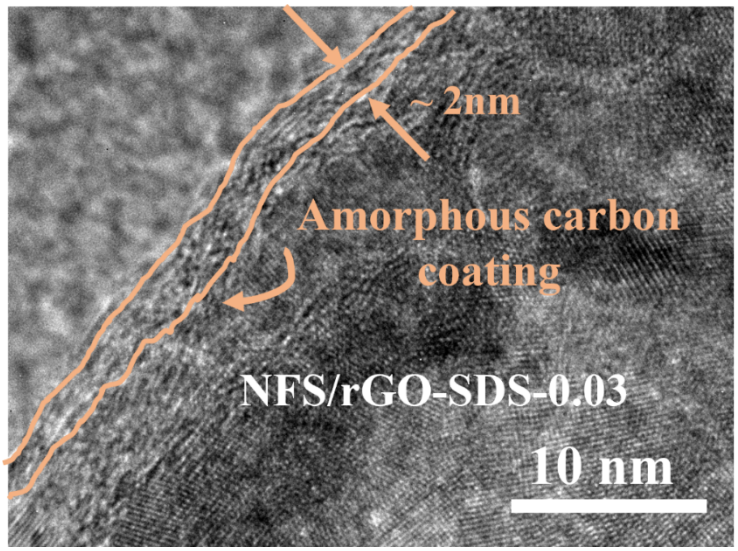

Fig. S8. HRTEM image of NFS/rGO-SDS-0.03, showing the amorphous carbon shell and its representative thickness.

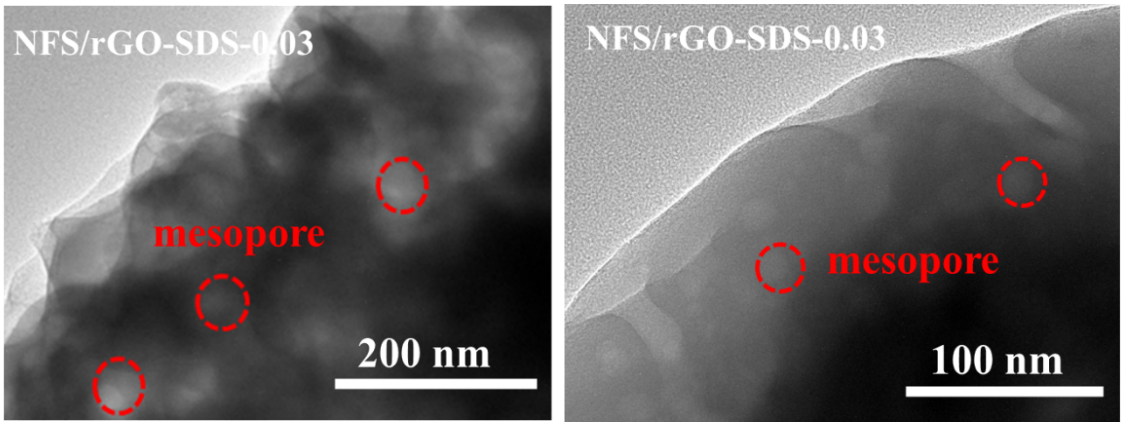

Fig. S9. TEM images of NFS/rGO-SDS-0.03.

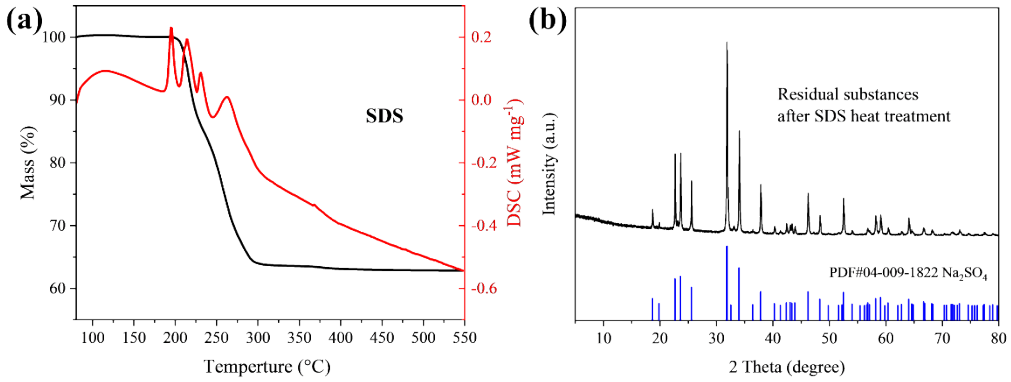

Fig. S10. (a) TG-DSC curves of SDS, showing that the main mass-loss/decomposition stage occurs within approximately 200-300 °C; (b) XRD pattern of the residue obtained after thermal treatment of pure SDS under the same heating conditions, indicating Na_2SO_4 as the dominant crystalline residue.

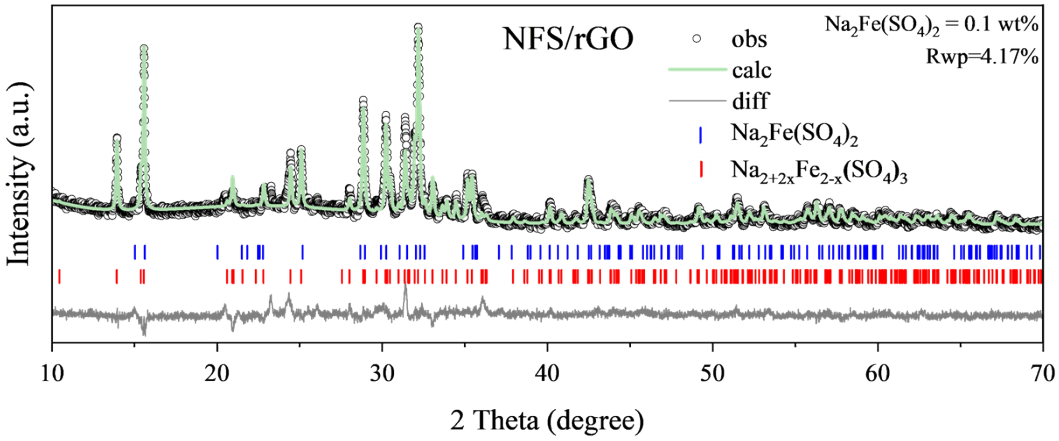

Fig. S11. Rietveld refinement XRD pattern of NFS/rGO, with the refined minor $Na_2Fe(SO_4)_2$ heterophase fraction labelled in the figure.

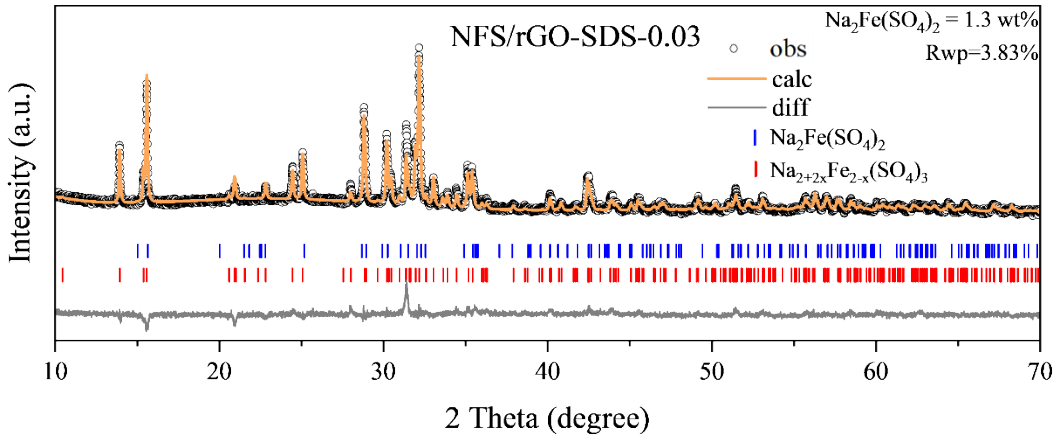

Fig. S12. Rietveld refinement XRD pattern of NFS/rGO-SDS-0.03, with the refined minor $Na_2Fe(SO_4)_2$ heterophase fraction labelled in the figure.

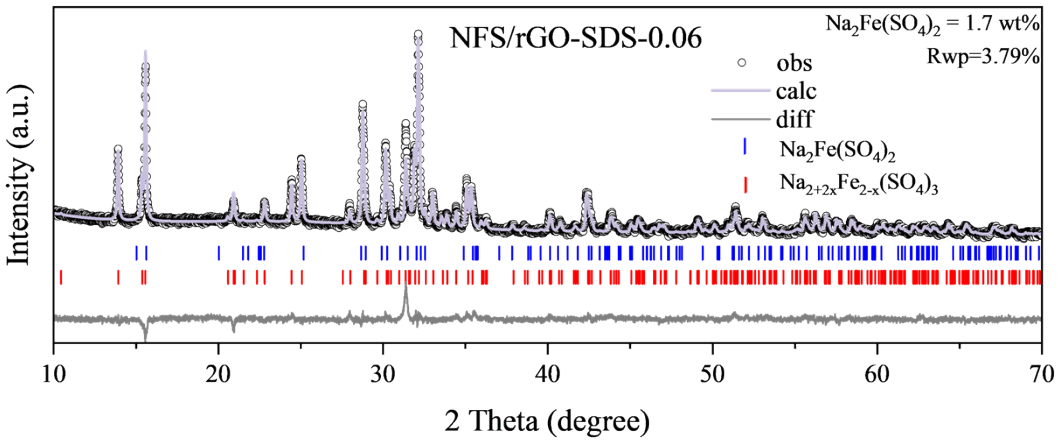

Fig. S13. Rietveld refinement XRD pattern of NFS/rGO-SDS-0.06, with the refined minor $Na_2Fe(SO_4)_2$ heterophase fraction labelled in the figure.

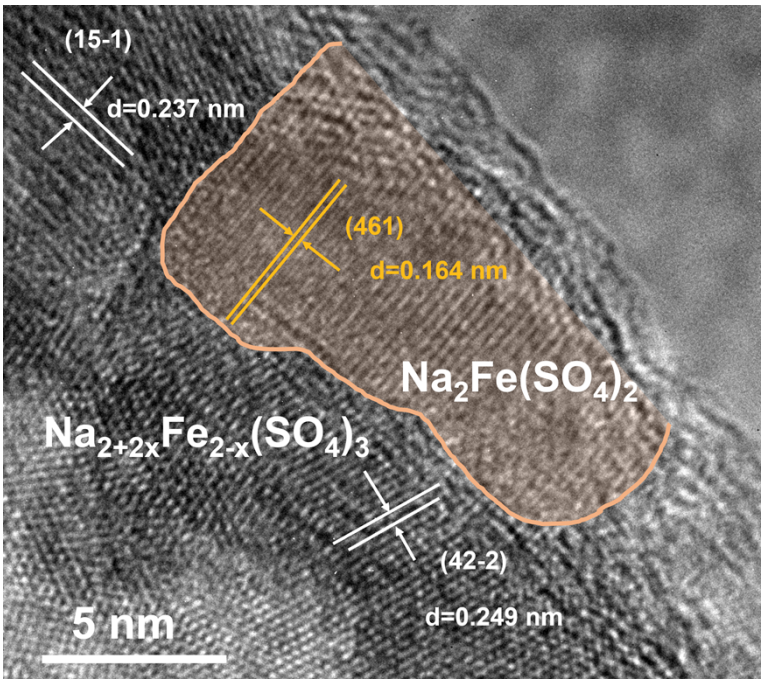

Fig. S14. HRTEM image of NFS/rGO-SDS-0.03 focusing on the internal crystalline region, specifically highlighting the lattice fringes of the metastable $Na_2Fe(SO_4)_2$ heterophase and its distinct boundaries with the main alluaudite matrix.

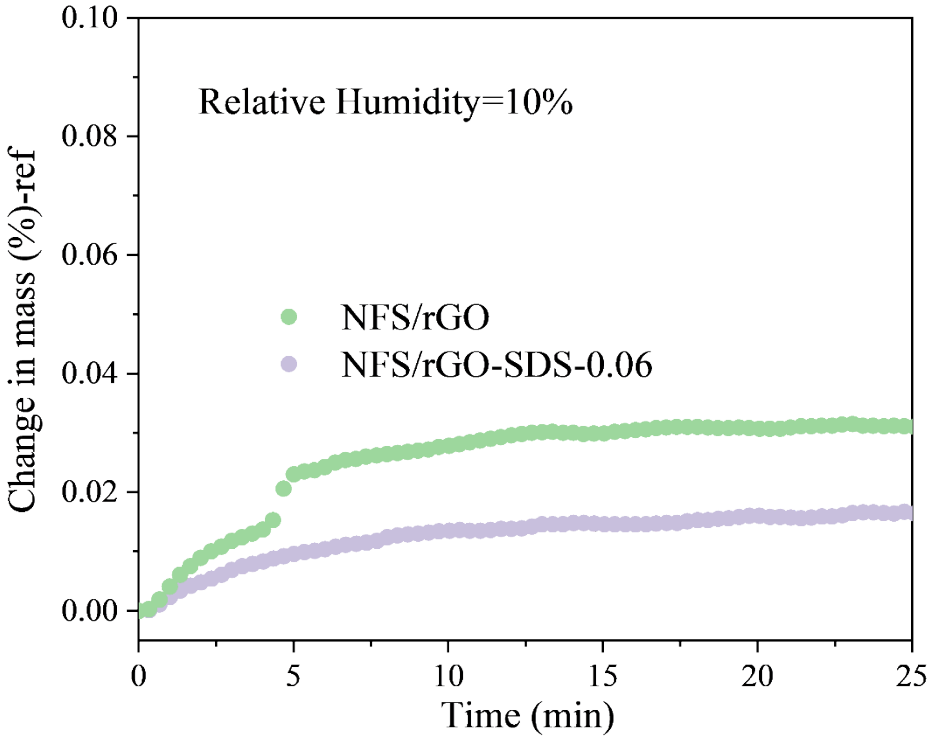

Fig. S15. Moisture sorption kinetics test conducted at 10% RH, terminated when $dm/dt < 0.002\%\ min^{-1}$.

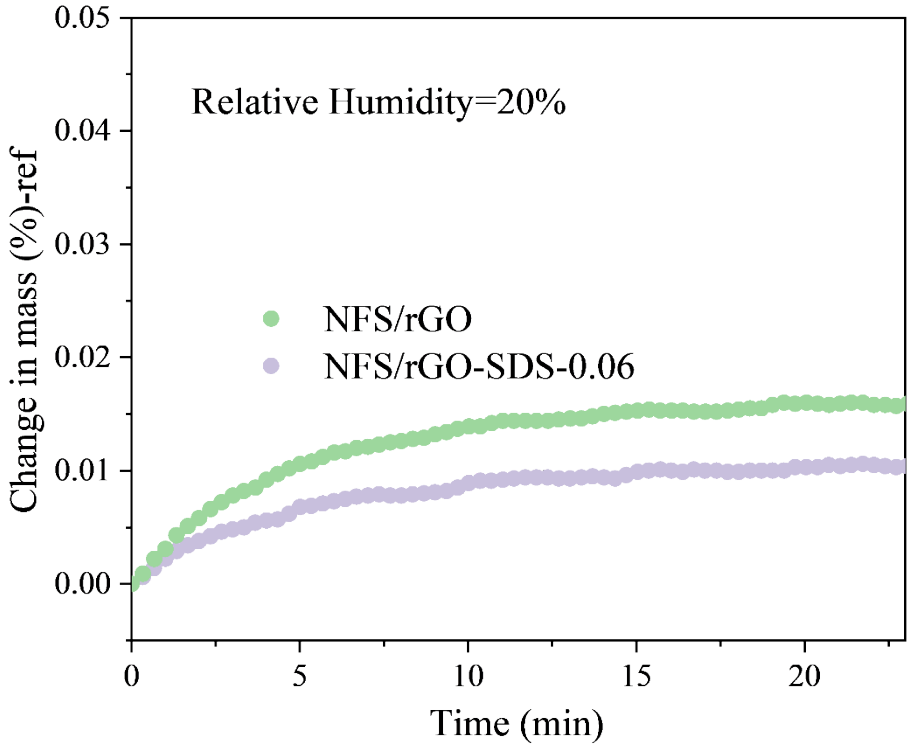

Fig. S16. Moisture sorption kinetics test conducted at 20% RH, terminated when $dm/dt < 0.002\%\ min^{-1}$.

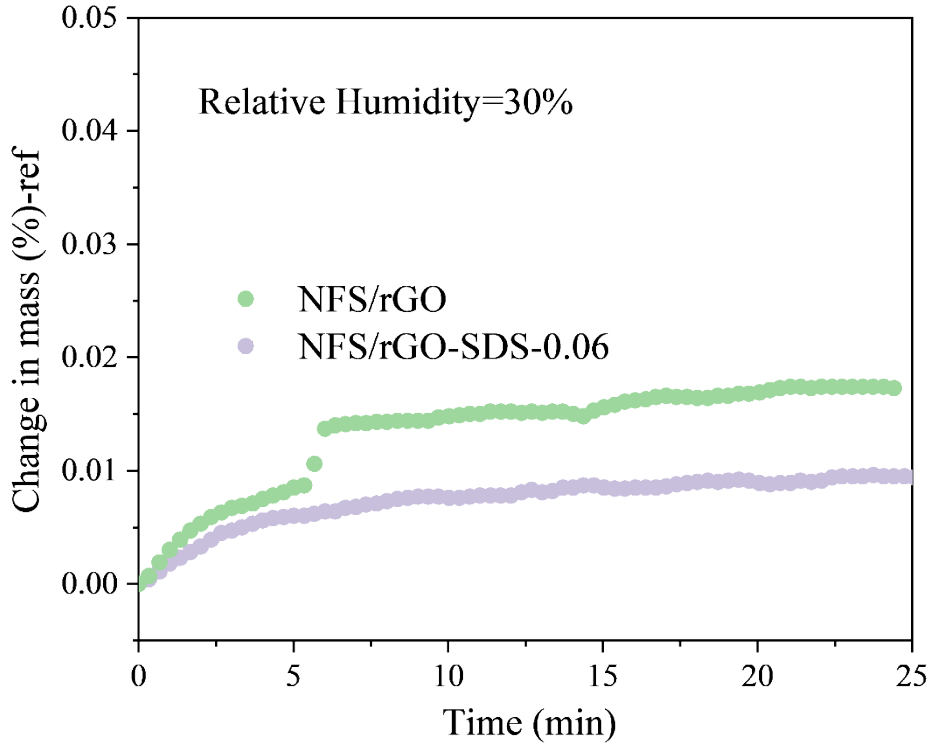

Fig. S17. Moisture sorption kinetics test conducted at 30% RH, terminated when $dm/dt < 0.002\%\ min^{-1}$.

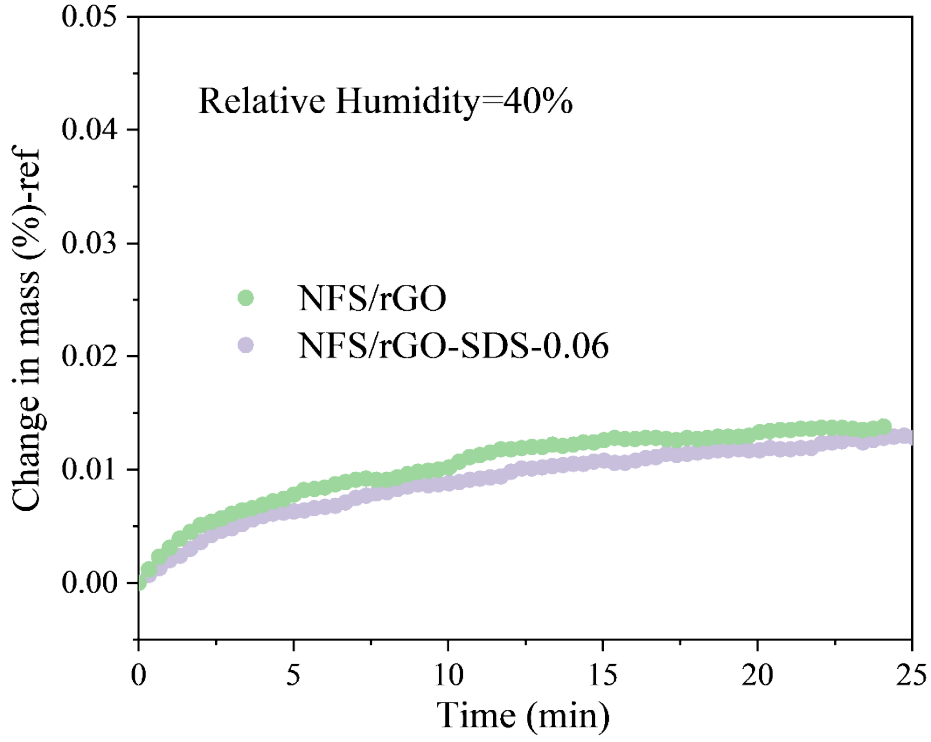

Fig. S18. Moisture sorption kinetics test conducted at 40% RH, terminated when $dm/dt < 0.002\%\ min^{-1}$.

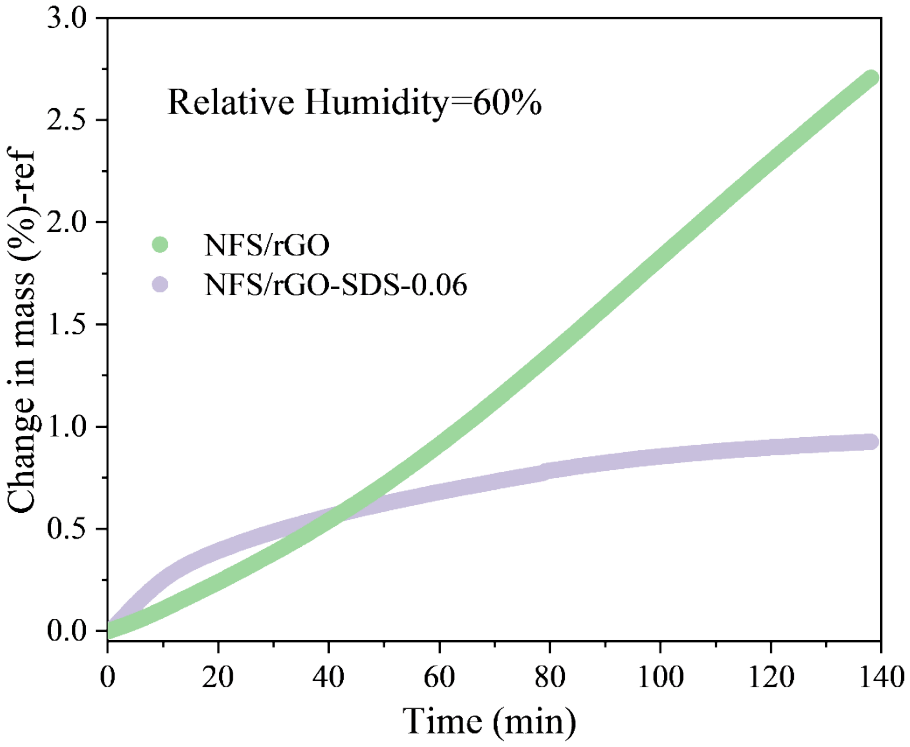

Fig. S19. Moisture sorption kinetics test conducted at 60% RH.

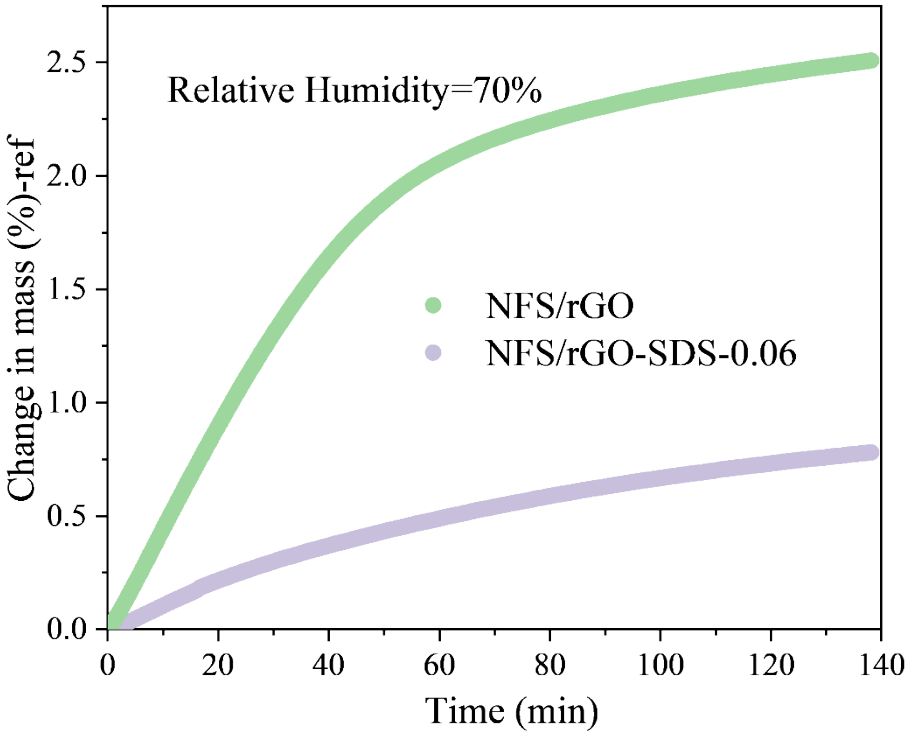

Fig. S20. Moisture sorption kinetics test conducted at 70% RH.

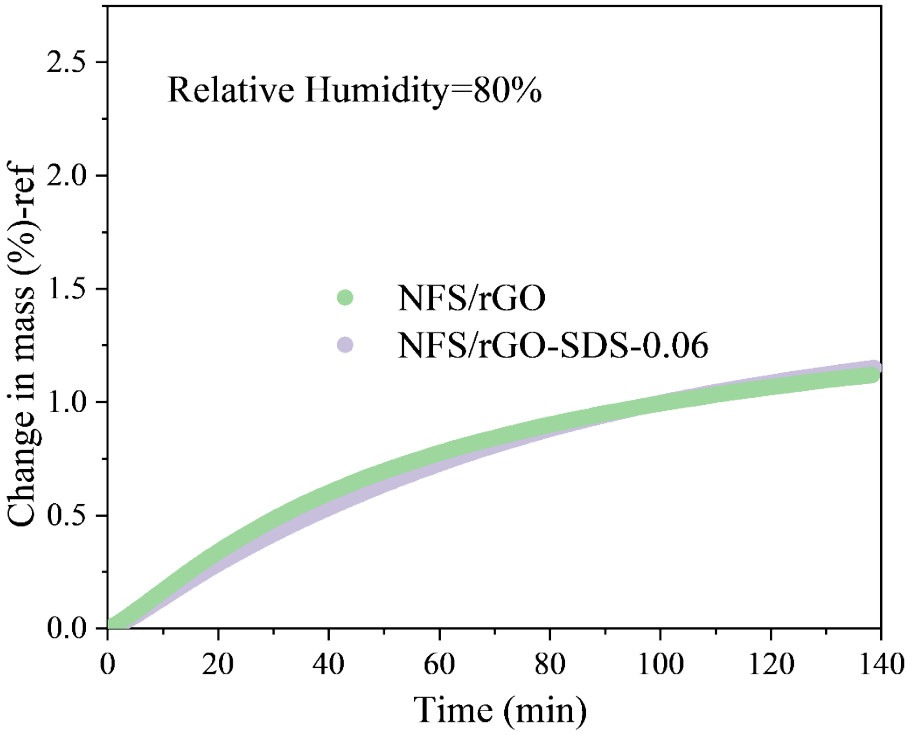

Fig. S21. Moisture sorption kinetics test conducted at 80% RH.

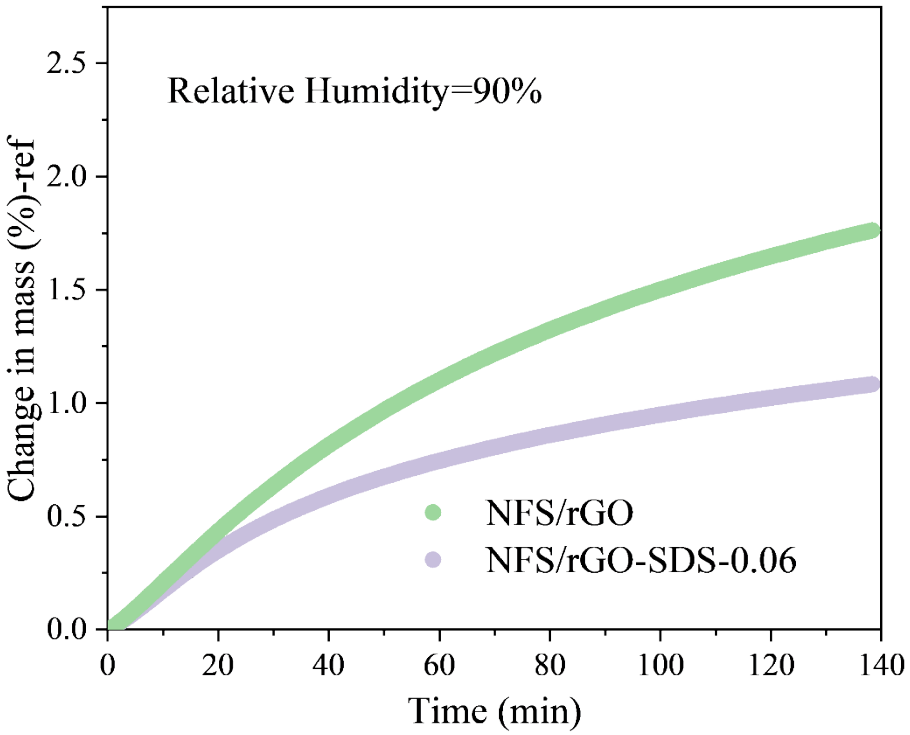

Fig. S22. Moisture sorption kinetics test conducted at 90% RH.

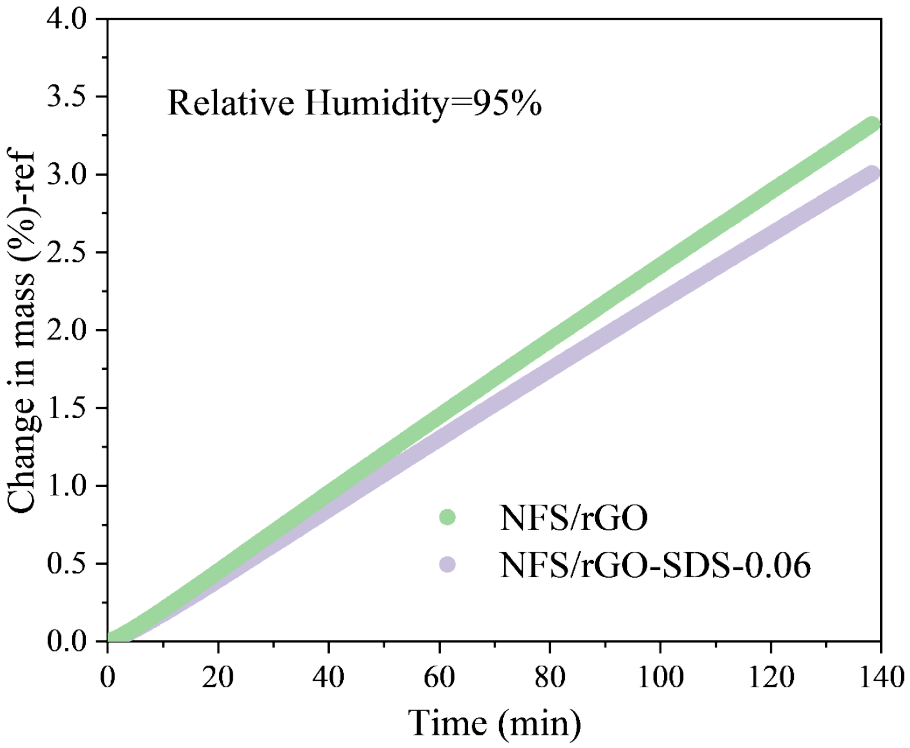

Fig. S23. Moisture sorption kinetics test conducted at 95% RH.

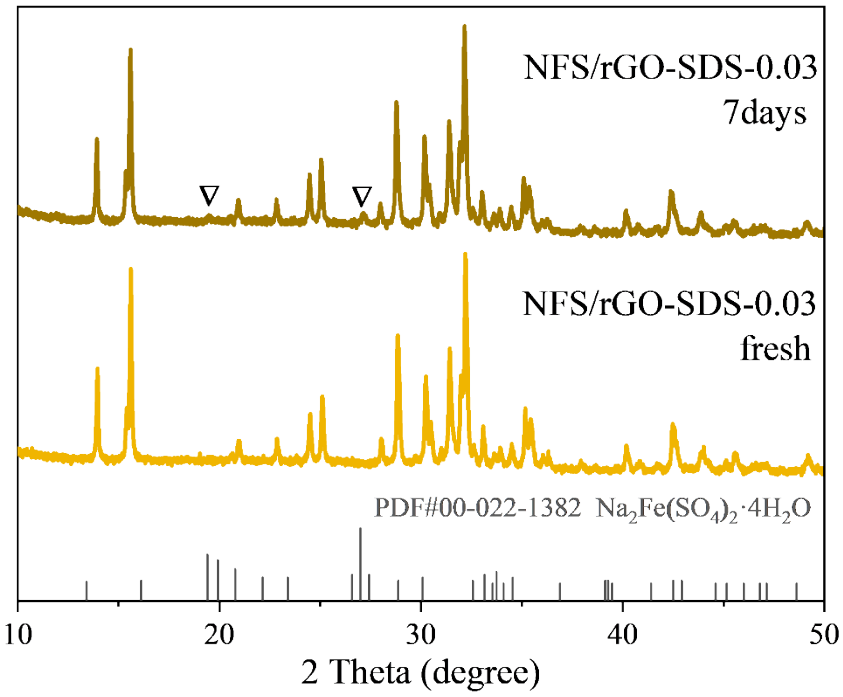

Fig. S24. XRD pattern evolution of NFS/rGO-SDS-0.03 exposed to ambient air for 7 days.

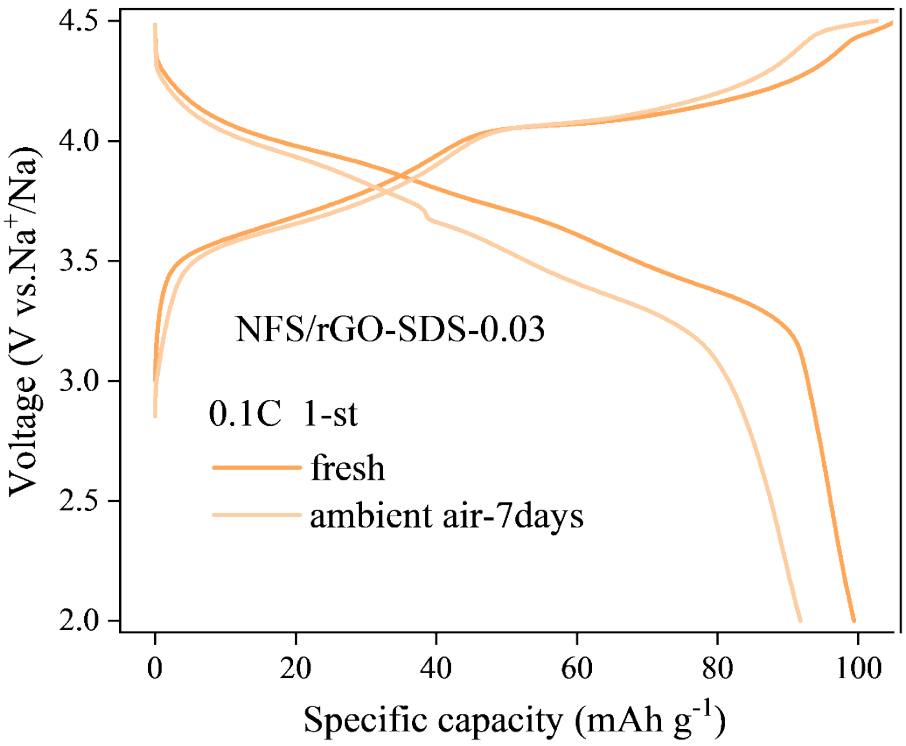

Fig. S25. Comparison of charge-discharge curves between the fresh NFS/rGO-SDS-0.03 sample and the sample exposed to ambient air for 7 days.

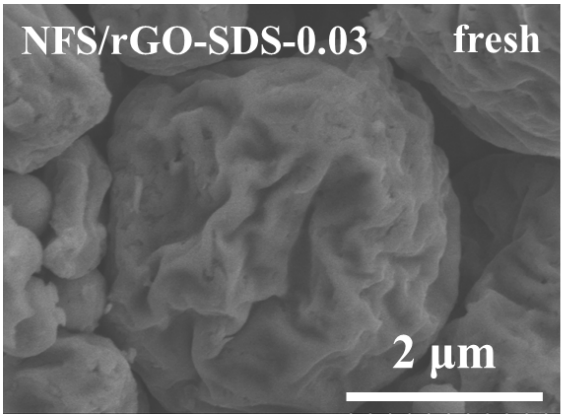

Fig. S26. SEM image of the fresh NFS/rGO-SDS-0.03 sample.

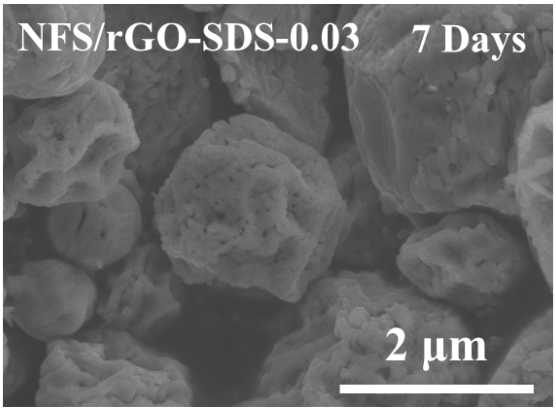

Fig. S27. SEM image of NFS/rGO-SDS-0.03 after exposure to air for 7 days.

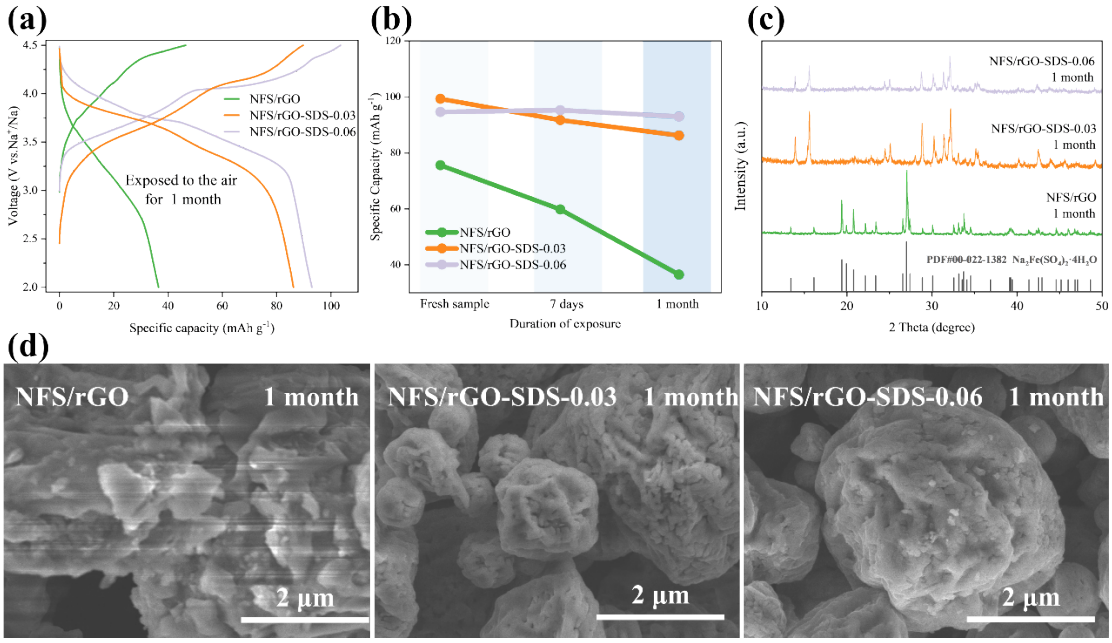

Fig. S28. Electrochemical performance, capacity retention, XRD patterns, and SEM images of NFS/rGO, NFS/rGO-SDS-0.03, and NFS/rGO-SDS-0.06 after exposure to ambient air with a relative humidity of approximately 55%RH for one month.

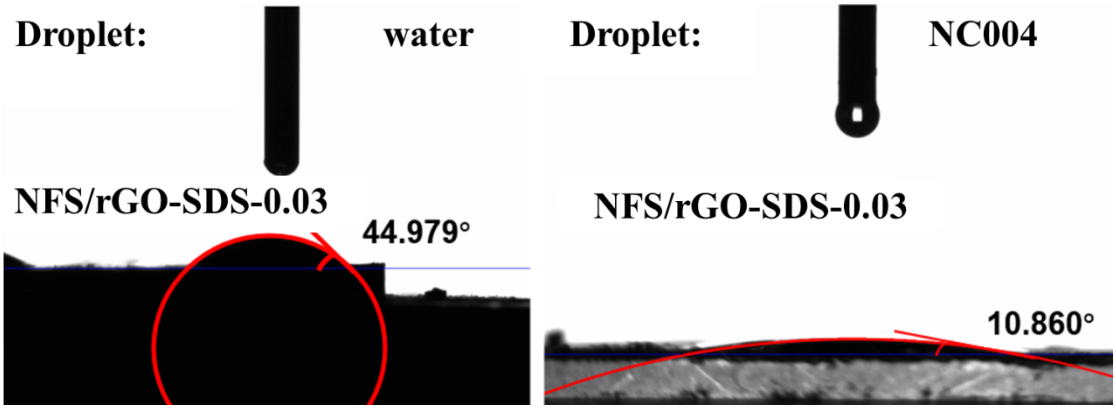

Fig. S29. Contact angle measurement images of NFS/rGO-SDS-0.03 toward water and electrolyte NC004.

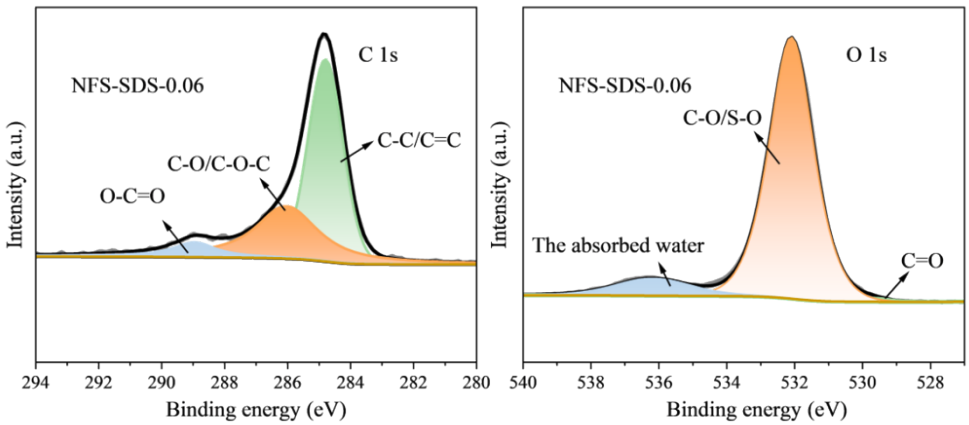

Fig. S30. High-resolution XPS spectra of C 1s and O 1s for NFS-SDS-0.06.

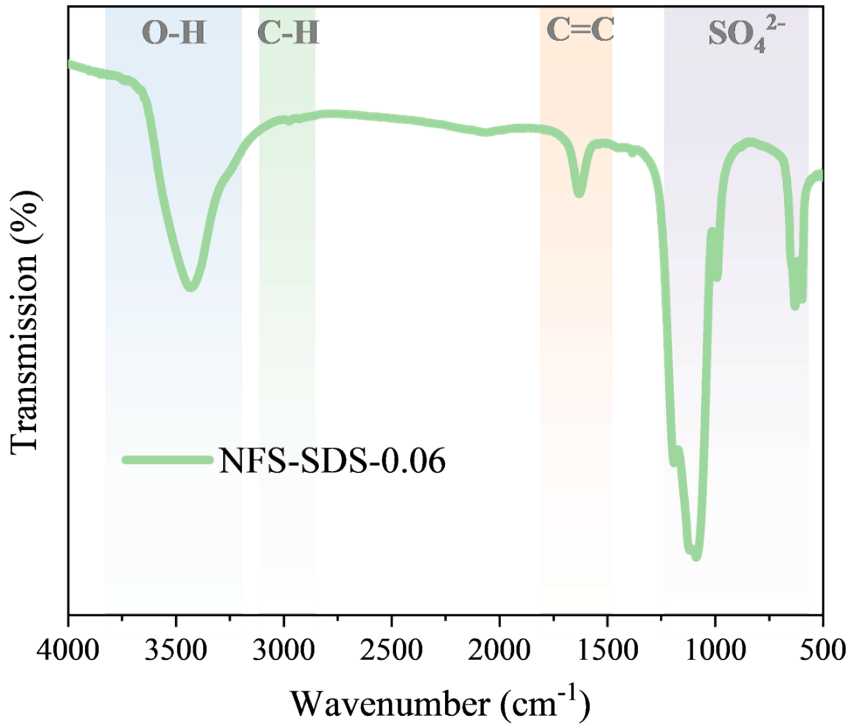

Fig. S31. FT-IR spectrum of the NFS-SDS-0.06.

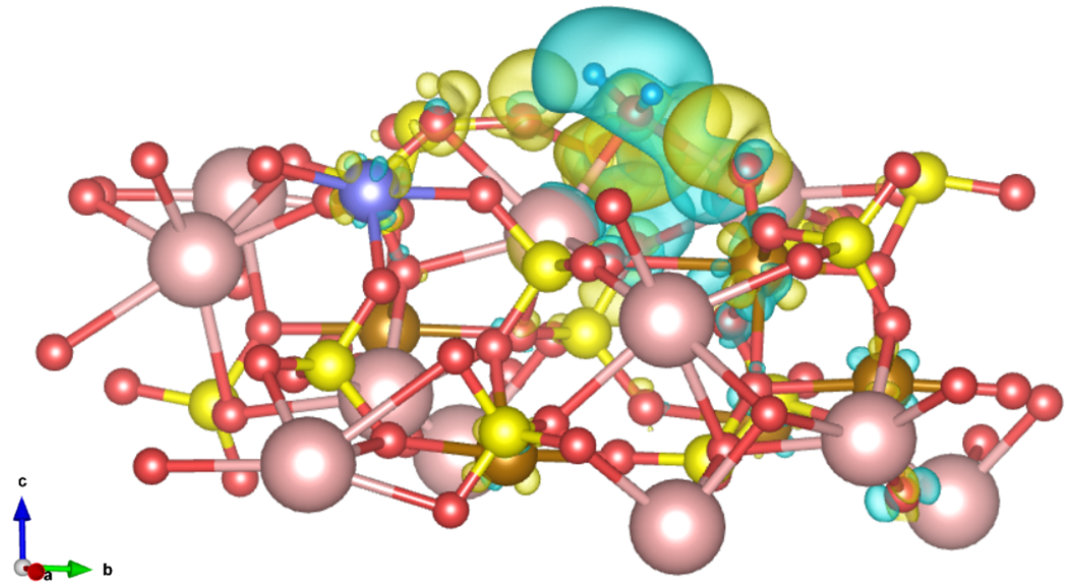

Fig. S32. Computational model of H_2O adsorption energy on bare NFS (NFS|H_2O).

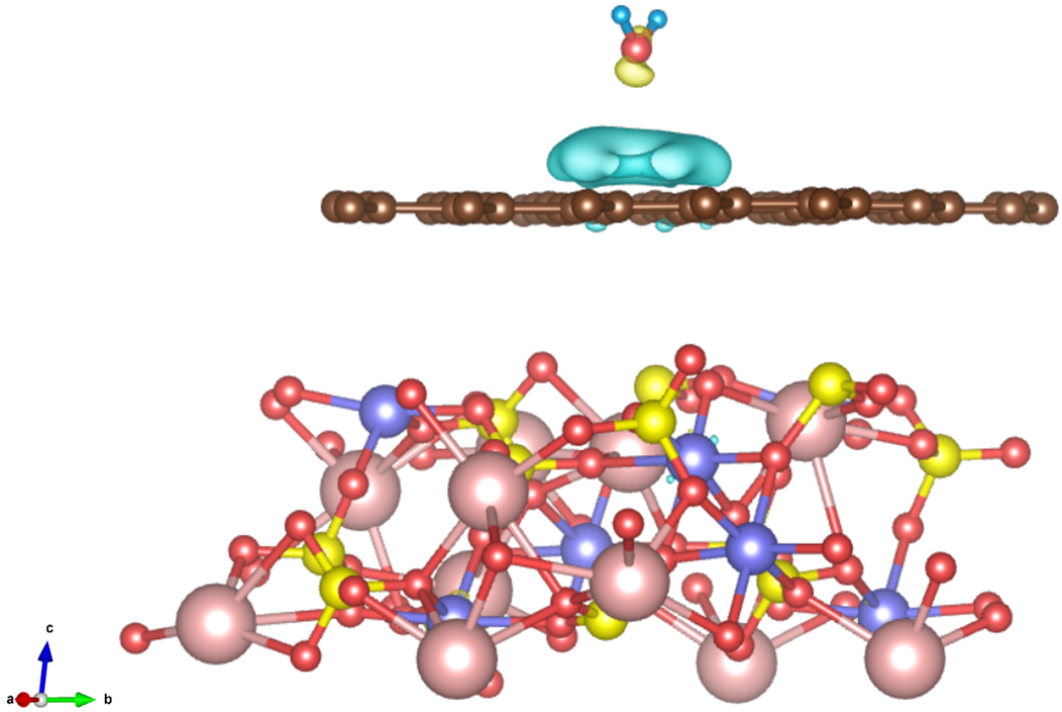

Fig. S33. Computational model of H_2O adsorption energy on the perfect graphite/NFS interface (NFS@G|H_2O).

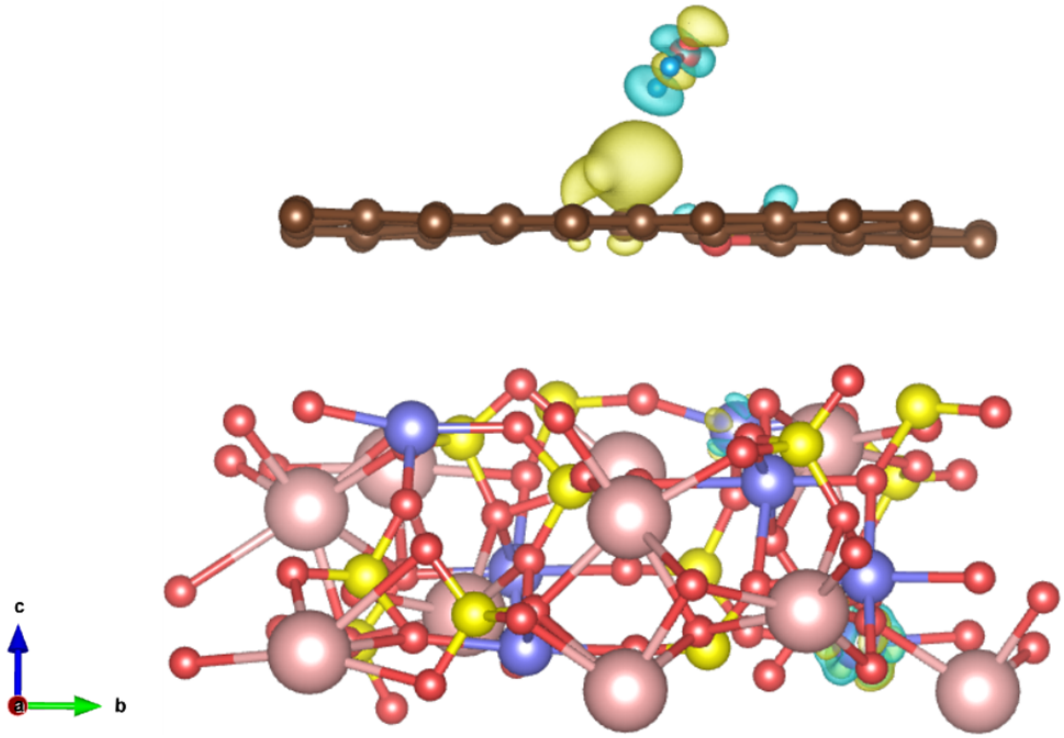

Fig. S34. Computational model of H_2O adsorption energy on the oxygen-containing defective graphite/NFS interface (NFS@G-O|H_2O).

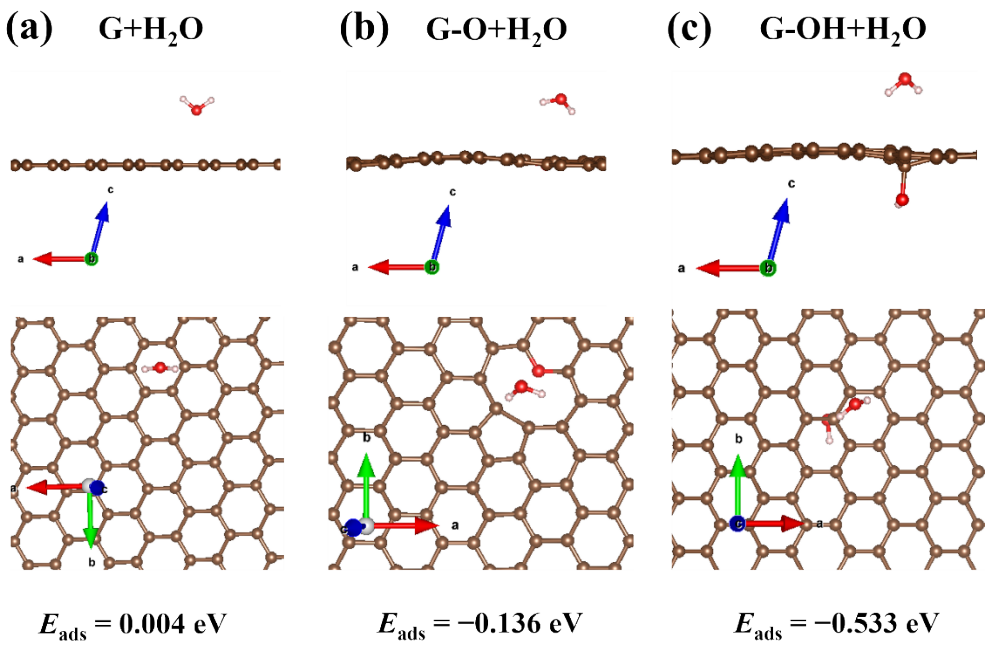

Fig. S35. Optimized H_2O adsorption configurations and calculated adsorption energies on carbon-only surfaces with different surface states: (a) pristine carbon, (b) carbonyl-containing carbon, and (c) hydroxyl-functionalized carbon. The upper and lower panels show the side and top views, respectively. Brown, red, and white spheres represent C, O, and H atoms, respectively.

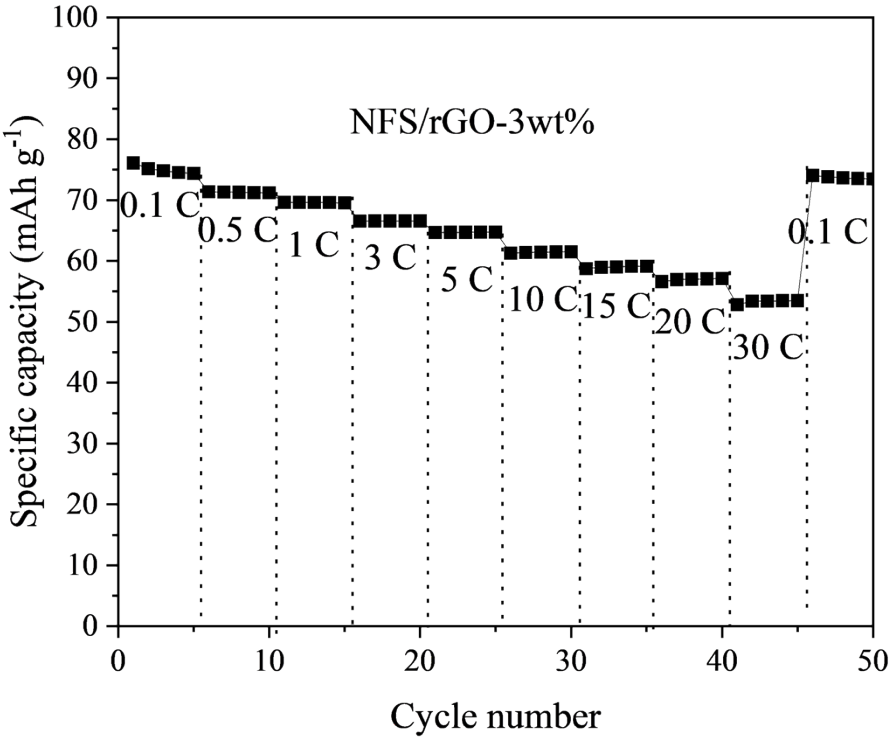

Fig. S36. Rate performance of the carbon-matched control sample (NFS/rGO-3 wt%), where the GO content was increased to achieve a carbon load of ~3 wt%.

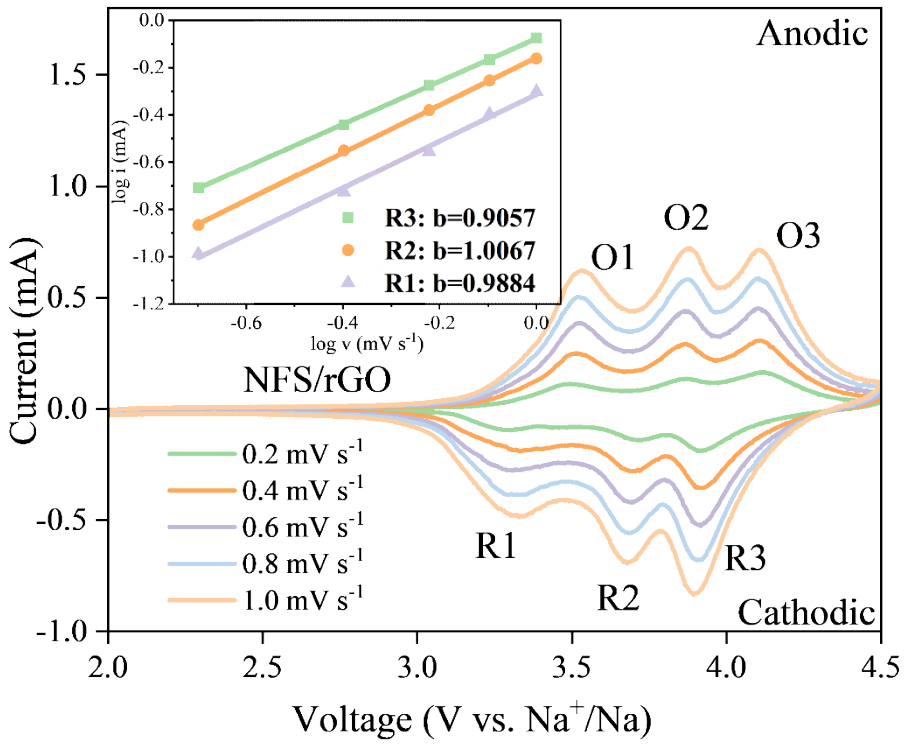

Fig. S37. CV curves of NFS/rGO at different scan rates, with the inset showing the *b*-value fitting curve and corresponding values.

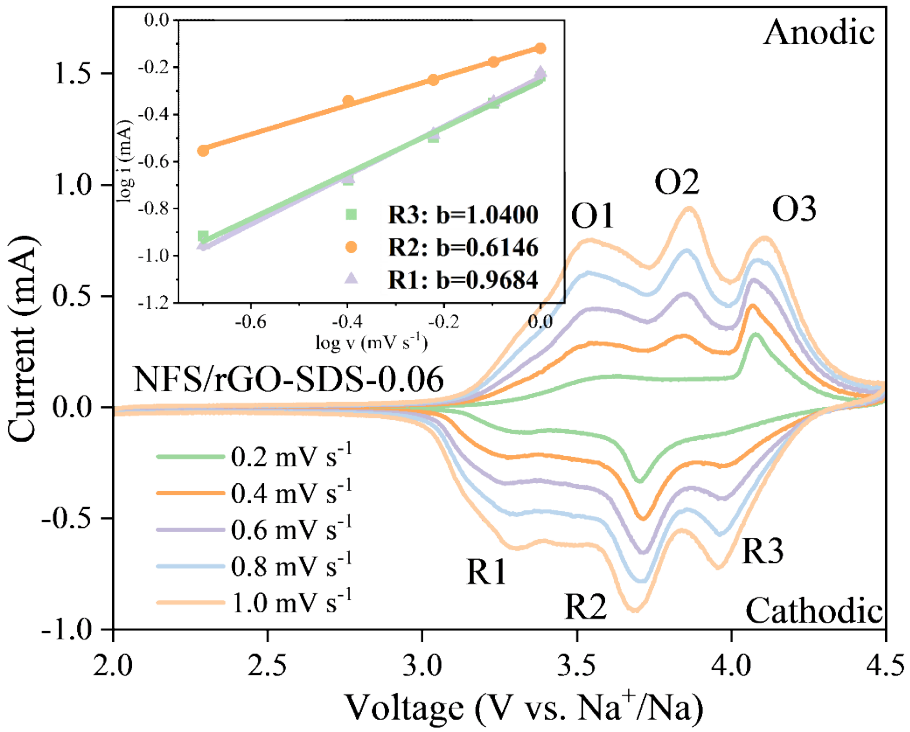

Fig. S38. CV curves of NFS/rGO-SDS-0.06 at different scan rates, with the inset showing the *b*-value fitting curve and corresponding values.

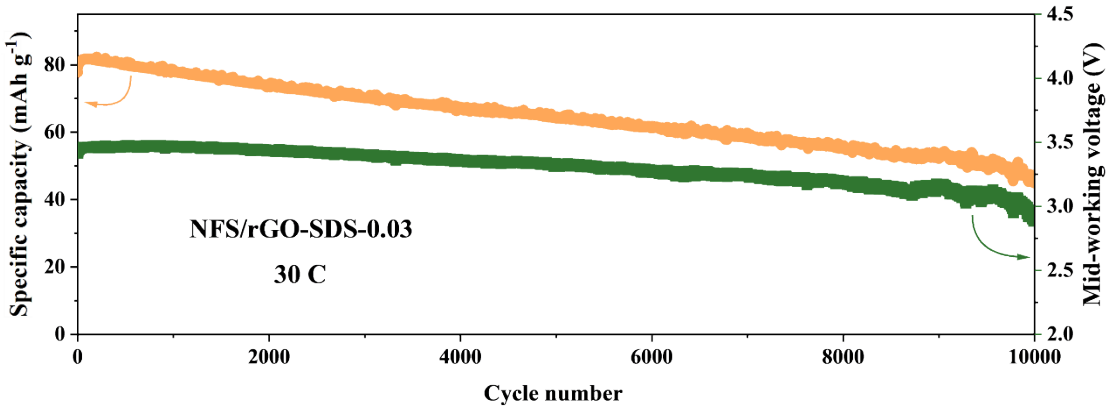

Fig. S39. Ultralong cycling performance of NFS/rGO-SDS-0.03 at 30 C for 10000 cycles.

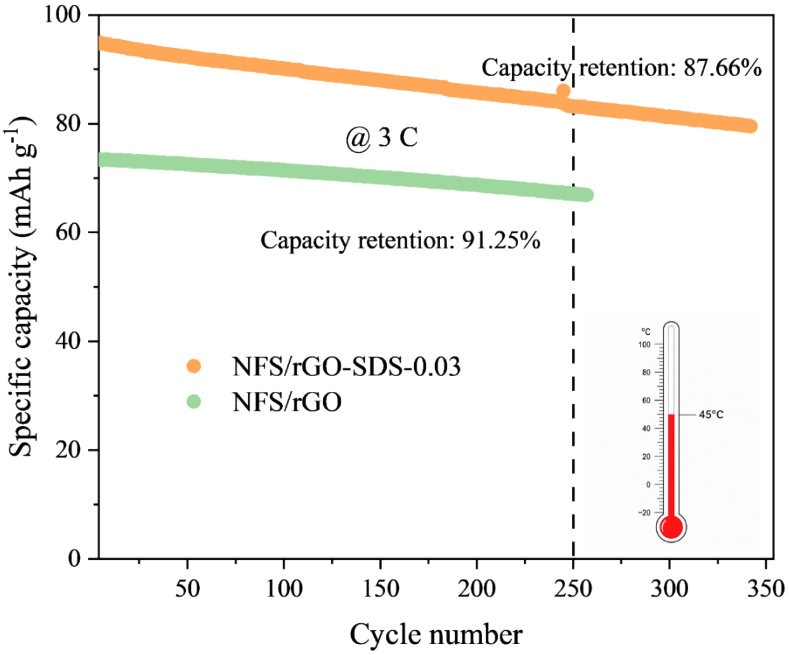

Fig. S40. Cycling performance of NFS/rGO and NFS/rGO-SDS-0.03 at 45 °C under 3 C.

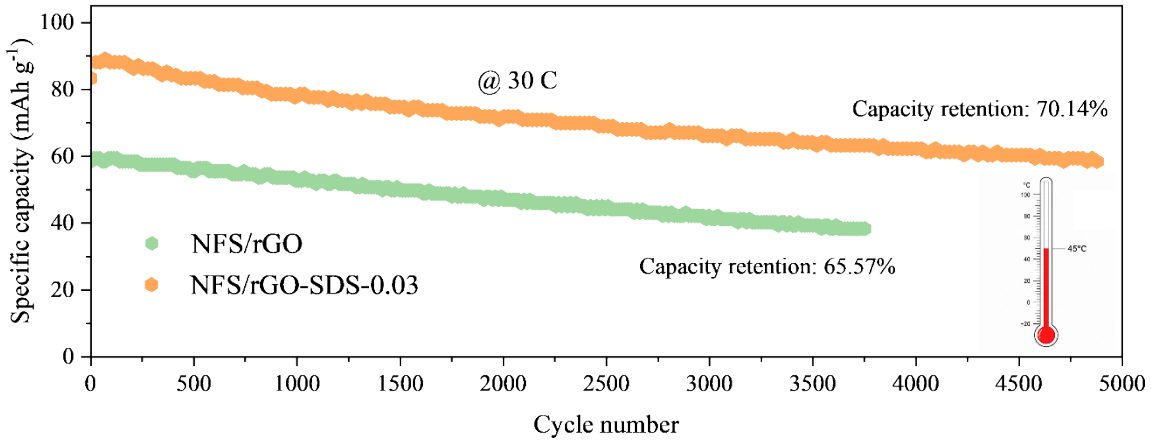

Fig. S41. Cycling performance of NFS/rGO and NFS/rGO-SDS-0.03 at 45 °C under 30 C.

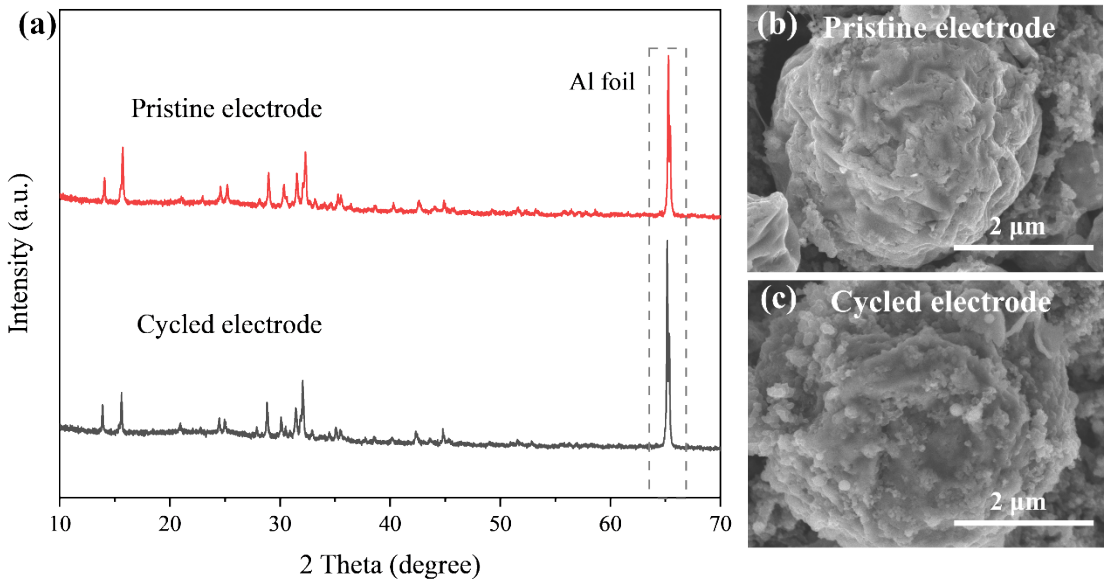

Fig. S42. *Ex situ* XRD patterns and SEM images of the NFS/rGO-SDS-0.03 electrode before and after cycling. (a) XRD patterns of the pristine and cycled electrodes. SEM images of the (b) pristine and (c) cycled electrodes.

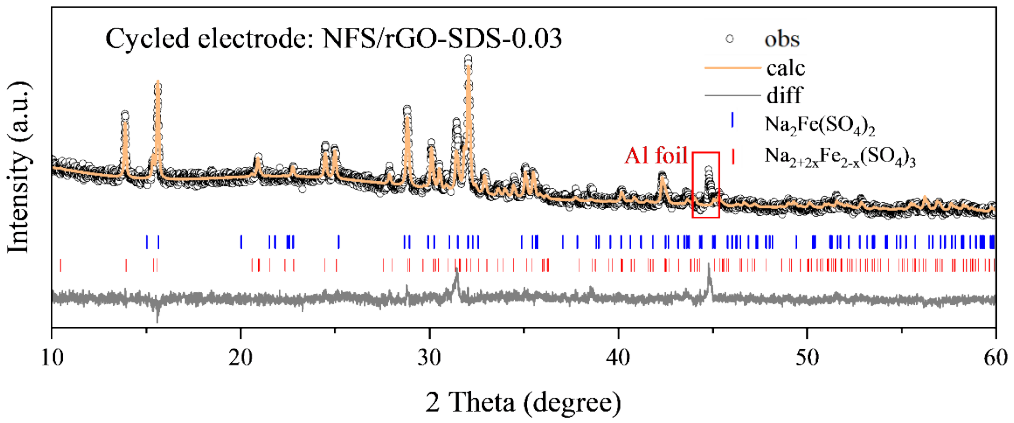

Fig. S43. Rietveld refinement of the *ex situ* XRD pattern of the cycled NFS/rGO-SDS-0.03 electrode.

Table S1. Atomic percentages obtained from EDS elemental mapping

Elements	NFS/rGO	NFS/rGO-SDS-0.03	NFS/rGO-SDS-0.06
O	54.4	46.2	48.3
C	22.4	24.8	24.3
S	9.5	12.0	10.9
Na	7.1	8.7	8.9
Fe	6.6	8.2	7.6
Na/Fe	1.08	1.06	1.17

Table S2. Four-point probe resistivity test results

	NFS/rGO	NFS/rGO-SDS-0.03	NFS/rGO-SDS-0.06
Volume Resistivity (Ω·cm)	Open Circuit	88.98	71.68

Table S3. BET measurement data

	NFS/rGO	NFS/rGO-SDS-0.03	NFS/rGO-SDS-0.06
BET Surface Area ($m^2 g^{-1}$)	7.54	11.67	12.87
Total pore volume of pores ($cm^3 g^{-1}$)	0.036	0.045	0.057
BJH Desorption average pore diameter (4V/A) (nm)	8.67	4.55	6.40

Table S4. XPS C 1s high-resolution spectrum and its corresponding components

Chemical species (at%)	NFS/rGO	NFS/rGO-SDS-0.03	NFS/rGO-SDS-0.06
C-C (sp^2)	15.83	16.25	17.71
C-C (sp^3)	10.68	6.70	6.62
C-O/C-O-C	6.28	6.54	6.63
O-C=O	4.96	4.82	2.31

Table S5. Atomic parameters of $Na_{2+2x}Fe_{2-x}(SO_4)_3$ refined from XRD Rietveld refinement of NFS/rGO.

Formula			NFS/rGO		
Crystal system			Monoclinic		
Space group			C1 2/c		
a (Å)			12.65946		
b (Å)			12.76448		
c (Å)			6.51126		
β (º)			115.55614		
Unit cell volume (Å^3)			949.223		
Atom	x	y	z	Occ.	Mult
S1	0.50000	0.21433	0.75000	0.500	4
Na1	0.27475	0.34519	0.37050	0.124	8
Fe	0.27475	0.34519	0.37050	0.876	8
O1	0.08202	0.31139	0.10664	1.000	8
O2	0.05621	0.19707	0.47295	1.000	8
S2	0.23072	0.10439	0.11060	1.000	8
O3	0.28452	0.16393	0.37857	1.000	8
O4	0.16901	0.01736	0.08692	1.000	8
O5	0.29860	0.35126	-0.00373	1.000	8
O6	0.53381	-0.01664	0.50508	1.000	8
Na2	0.00000	0.74576	0.25000	0.500	4
Na3	0.35711	0.07913	0.12902	0.681	8
Na4	-0.01765	0.07968	0.07728	0.453	8

Table S6. Atomic parameters of $Na_{2+2x}Fe_{2-x}(SO_4)_3$ refined from XRD Rietveld refinement of NFS/rGO-SDS-0.03.

Formula			NFS/rGO-SDS-0.03		
Crystal system			Monoclinic		
Space group			C1 2/c		
a (Å)			12.66910		
b (Å)			12.78410		
c (Å)			6.52392		
β (º)			115.54768		
Unit cell volume (Å^3)			953.324		
Atom	x	y	z	Occ.	Mult
S1	0.50000	0.22050	0.75000	0.500	4
Na1	0.27339	0.34416	0.37105	0.146	8
Fe	0.27339	0.34416	0.37105	0.854	8
O1	0.08856	0.31721	0.12658	1.000	8
O2	0.03622	0.19616	0.47445	1.000	8
S2	0.23028	0.10015	0.11400	1.000	8
O3	0.29697	0.16751	0.39800	1.000	8
O4	0.17046	0.01189	0.09997	1.000	8
O5	0.28665	0.35062	-0.00797	1.000	8
O6	0.53391	-0.01441	0.48153	1.000	8
Na2	0.00000	0.74557	0.25000	0.500	4
Na3	0.35856	0.08985	0.11584	0.703	8
Na4	-0.04682	0.08063	0.05973	0.495	8

Table S7. Atomic parameters of $Na_{2+2x}Fe_{2-x}(SO_4)_3$ refined from XRD Rietveld refinement of NFS/rGO-SDS-0.06.

Formula			NFS/rGO-SDS-0.06		
Crystal system			Monoclinic		
Space group			C1 2/c		
a (Å)			12.67619		
b (Å)			12.79892		
c (Å)			6.53525		
β (º)			115.56546		
Unit cell volume (Å^3)			956.479		
Atom	x	y	z	Occ.	Mult
S1	0.50000	0.22275	0.75000	0.500	4
Na1	0.27364	0.34467	0.37133	0.144	8
Fe	0.27364	0.34467	0.37133	0.856	8
O1	0.09101	0.31758	0.13270	1.000	8
O2	0.03173	0.19520	0.47322	1.000	8
S2	0.23155	0.10061	0.11483	1.000	8
O3	0.30421	0.17541	0.41100	1.000	8
O4	0.17214	0.01459	0.09683	1.000	8
O5	0.28678	0.35304	0.00028	1.000	8
O6	0.53284	-0.01353	0.46978	1.000	8
Na2	0.0000	074767	0.25000	0.500	4
Na3	0.35372	0.08915	0.10839	0.686	8
Na4	-0.05780	0.07930	0.05007	0.494	8

Table S8. DFT calculation results: formation energies of various structural model

Structural model	Formation Energy (E_f) (eV nm^{-2})
NFS@G	-0.12
NFS@G-O	0.15
NFS@G-OH	-0.32

Table S9. DFT calculation results: adsorption energies of water molecules on various structural model

Structural model	Adsorption Energy (E_{ads}) (eV)
NFS|H_2O	-0.79
NFS@G|H_2O	-0.02
NFS@G-O|H_2O	-0.43
NFS@G-OH|H_2O	-0.06
G|H_2O	0.004
G-O|H_2O	-0.136
G-OH|H_2O	-0.533

Note: G, G–O, and G–OH denote pristine carbon, carbonyl-containing carbon, and hydroxyl-functionalized carbon, respectively. NFS@G, NFS@G–O, and NFS@G–OH represent NFS surfaces covered by the corresponding carbon layers.

Table S10. EIS fitting parameters of NFS/rGO, NFS/rGO-SDS-0.03, and NFS/rGO-SDS-0.06

Sample	R_{st} (Ω)	R_{ct} (Ω)
NFS/rGO	5.513	661.3
NFS/rGO-SDS-0.03	4.750	348.1
NFS/rGO-SDS-0.06	4.685	517.4

Table S11. Calculated contribution ratios of capacitive and diffusion-controlled behaviors for NFS/rGO at different scan rates

Scan rate (mV s^{-1})	Diffusion	Capacitive
0.2	0.0743	0.9257
0.4	0.0554	0.9446
0.6	0.0455	0.9555
0.8	0.0419	0.9581
1.0	0.0319	0.9681

Table S12. Calculated contribution ratios of capacitive and diffusion-controlled behaviors for NFS/rGO-SDS-0.03 at different scan rates

Scan rate (mV s^{-1})	Diffusion	Capacitive
0.2	0.093	0.9063
0.4	0.0737	0.9263
0.6	0.0605	0.9395
0.8	0.0515	0.9485
1.0	0.0420	0.9580

Table S13. Calculated contribution ratios of capacitive and diffusion-controlled behaviors for NFS/rGO-SDS-0.06 at different scan rates

Scan rate (mV s^{-1})	Diffusion	Capacitive
0.2	0.1101	0.8899
0.4	0.0890	0.9110
0.6	0.0719	0.9281
0.8	0.0619	0.9381
1.0	0.0522	0.9478

Table S14. Comparison of representative sodium iron sulfate cathodes

Cathode	Voltage (V)	Capacity (mAh g^{-1})	Cycling stability	Environmental stability
$Na_2Fe_2(SO_4)_3$ [S1]	~3.8	101 (0.05C); 54 (20C)	Not reported	Not reported
NFS@C@2%CNTs [S2]	~3.5	95.9 (0.05C); 60 (10C)	94.7% after 250 cycles at 2 C	Not reported
$Na_{2.5}Fe_{1.75}(SO_4)_3$/C [S3]	~3.8	107.6 (0.1C); 65.3 (10C)	65.9% after 200 cycles at 1 C	Not reported
$Na_{2+2\delta}Fe_{2-\delta}(SO_4)_3$/C [S4]	3.75	82.0 (0.05C); 54 (10C)	92.2% after 1000 cycles at 10 C	Not reported
$Na_{2.26}Fe_{1.87}(SO_4)_3$/rGO [S5]	~3.7	96 (0.05C); 80 (10C)	65.32% after ~5600 cycles at 5 C	Not reported
$Na_{2.72}Fe_{1.64}(SO_4)_3$/FG [S6]	~3.8	110 (0.1C); 79 (15C)	80.7% after 15000 cycles at 15 C	Not reported
$Na_{2.4}Fe_{1.8}(SO_4)_3$/rGO [S7]	3.75	100 (0.05C); 54 (30C)	58% after 10000 cycles at 10 C	Not reported
$Na_{2.60}Fe_{1.70}(SO_4)_3$/rGO [S8]	3.74	80 (0.1C); 45 (10C)	73% after 500 cycles at 8 C	Not reported
$Na_2Fe_2(SO_4)_3$/C/rGO [S9]	3.75	107.9 (0.1C); 75.1 (10C)	80.1% after 800 cycles at 5 C	Not reported
$Na_8Fe_5(SO_4)_9$/rGO [S10]	3.8	102.2 (0.2C); 63 (50C)	91.9% after 1000 cycles at 10 C	Not reported
$Na_6Fe_5(SO_4)_8$/CNTs [S11]	3.74	110.2 (0.1C); 86.4 (2C)	>100% after 1000 cycles at 2 C	Not reported
$Na_{2.5}Fe_2(SO_4)_{2.5}(PO_4)_{0.5}$/KB [S12]	3.6	112 (0.2C); 79.5 (20C)	88.8% after 10,000 cycles at 10 C	1 week in air, ~60% RH; stable
$Na_{2.9}Fe_{1.7}(SO_4)_{2.7}(PO_4)_{0.3}$/AB [S13]	3.57	100.4 (0.1C); 86.7 (30C)	85.5% after 6000 cycles at 30 C	1 week in air, ~50% RH; stable
$Na_{2.466}Fe_{1.724}Mg_{0.043}(SO_4)_3$/rGO [S14]	3.74	102.2 (10 mA g^{-1}); 79.4 (2000 mA g^{-1})	70.8% after 5000 cycles at 500 mA g^{-1}	24 h at 45% RH; 11.2 mAh g^{-1} capacity drop
This work	**~3.8**	**102.3 (0.1C); 81.5 (30C)**	**80.0% after 5000 cycles at 30 C**	**1 week in air, ~50% RH; stable**

Reference

[S1] P. Barpanda, G. Oyama, S.-i. Nishimura, S.-C. Chung and A. Yamada, Nat. Commun., 2014, 5, 4358.

[S2] W. Yang, Q. Liu, L. Hou, Q. Yang, D. Mu, G. Tan, L. Li, R. Chen and F. Wu, Small, 2023, 20, 2306595.

[S3] Y. Liu, Y. Han, Z. Song, W. Song, Z. Miao, Y. Chen, J. Ding and W. Hu, ACS Appl. Mater. Interfaces, 2024, 16, 13828-13838.

[S4] W. Yang, Q. Liu, Q. Yang, S. Lu, W. He, L. Li, R. Chen and F. Wu, Energy Storage Mater., 2025, 74, 103925.

[S5] J. Zhang, Y. Yan, X. Wang, Y. Cui, Z. Zhang, S. Wang, Z. Xie, P. Yan and W. Chen, Nat. Commun., 2023, 14, 3701.

[S6] Q. Xiao, Y. Li, K. Wang, C. Ma, B. Liu and Y. Zhao, J. Mater. Chem. A, 2025, 13, 3727-3734.

[S7] Y. Fang, Q. Liu, X. Feng, W. Chen, X. Ai, L. Wang, L. Wang, Z. Ma, Y. Ren, H. Yang and Y. Cao, J. Energy Chem., 2021, 54, 564-570.

[S8] Y. Li, Y. Zhang, Y. Tang, J. Xie, W. Ma, L. Deng and L. Liu, Appl. Mater. Today, 2023, 35, 101966.

[S9] M. Chen, D. Cortie, Z. Hu, H. Jin, S. Wang, Q. Gu, W. Hua, E. Wang, W. Lai, L. Chen, S. L. Chou, X. L. Wang and S. X. Dou, Adv. Energy Mater., 2018, 8, 1800944.

[S10] C. Liu, K. Chen, H. Xiong, A. Zhao, H. Zhang, Q. Li, X. Ai, H. Yang, Y. Fang and Y. Cao, eScience, 2024, 4, 100186.

[S11] S. Li, X. Song, X. Kuai, W. Zhu, K. Tian, X. Li, M. Chen, S. Chou, J. Zhao and L. Gao, J. Mater. Chem. A, 2019, 7, 14656-14669.

[S12] C. Liu, K. Chen, F. Li, A. Zhao, P. Liu, Z. Chen, Y. Fang and Y. Cao, J. Am. Chem. Soc., 2025, 147, 14635-14646.

[S13] C. Liu, K. Chen, F. Li, A. Zhao, Z. Chen, Y. Fang and Y. Cao, Nano Energy, 2024, 125, 109557.

[S14] L. Wen, J. Zhang, J. Zhang, L. Zhao, X. Wang, S. Wang, S. Ma, W. Li, J. Luo, J. Ge and W. Chen, eScience, 2025, 5, 100313.